Carpathian Journal of Earth and Environmental Sciences, February 2020, Vol. 15, No. 1, p. 233 - 245; Doi:10.26471/cjees/2020/015/125

LINK DIAGENETIC CEMENTS CHARACTERISTICS TO THE PETROLEUM SOURCE AND FLUID EVOLUTION: AN EXAMPLE FROM THE EOCENE SHAHEJIE FORMATION, BOHAI BAY BASIN, CHINA

Zhiyong NI[1, 2*], Jianhui ZENG[1, 2], Xiaoxiao MAO[1, 2], Bing YOU[1, 2], Xuejun WANG[3] & Qing LIU[3]

[1]State Key Laboratory of Petroleum Resources and Prospecting, China University of Petroleum, Beijing 102249, China.
[2]College of Geosciences, China University of Petroleum, Beijing 102249, China.
[3]Shengli Oil field Branch Company, SINOPEC, Dongying, 257000, China.
** Corresponding author: Zhi-Yong Ni*
Mailing address: 18 Fuxue Road, Changping District, Beijing 102249, P.R. China
Tel: (+86)-10-8973-9110 Email: nizhy@cup.edu.cn

Abstract: The Dongying depression is one of the regions with the high petroleum production in the Bohai Bay basin. The third member of the Eocene Shahejie Formation (Es3, 42.5-38.0 Ma) is one of principal reservoir rock section in the region. This paper reports a new paleo-fluid dataset obtained from diagenetic cements, in an attempt to reveal the fluid source and evolution of the Shahejie Formation. The petrology, mineralogy, stable isotopic compositions, and fluid inclusions in carbonate cements in the Es3 sandstone reservoirs in the Dongying depression were investigated. Group I calcite cement display red luminescence. In contrast, Group II calcite cements have undergone dolomitization and is not luminescent. Furthermore, fluid inclusions in quartz overgrowth are characterized by low salinity (4.1%–4.8%), whereas Group II cement preserves high-salinity fluids (up to 22.6%). The C-O isotopic compositions of the carbonate cements are also distinct. The δ^{18}OPDB values of Group I and Group II range from –17.4‰ to –7.3‰ and –11.9‰ to –4.9‰, respectively. The carbon isotopic composition (δ^{13}CPDB) of Group II is more negative than that of Group I, and both are more negative than the lacustrine carbonates from the same basin. Our data suggest that Group I and Group II cements were produced from fluids derived from Es3 and Es4, respectively. Furthermore, the petroleum inclusions display two fluorescence colors (bright-yellow and khaki) under UV light. The homogenization temperatures of aqueous inclusions coexisting with two kinds of petroleum inclusions are consistent with each other. It suggests that the hydrocarbon fluid of the reservoir in Es3 was almost charged in the same time. The different fluorescence colors are caused by difference between source rocks. The integrated studies are useful to understand the fluid origin and evolution of the Eocene reservoir, and would improve the accuracy of reservoir prediction in Dongying depression.

Key words: C–O isotopes; fluid inclusions; carbonate cement; petroleum accumulation

1. INTRODUCTION

The Bohai Bay basin is one of the most important petroleum-rich basins in China, with nearly 30% of the total oil production of China (Hao et al., 2011). The Dongying depression is located in the Jiyang sub-basin, which is one of the most petroliferous regions. The upper part of Eocene Shaheje Formation (Es3) is one of the significant reservoirs, which is dominated by deltaic sandstones and show spatially heterogeneous oil-bearing properties (Hao et al., 2009a; Hao et al., 2011; Hao et al., 2009b; Huang & Pearson, 1999; Tian et al., 2017; Wang et al., 2016). The storage property of deep reservoirs is one of important factors to determine the oil-bearing property. In particular, the cementation and dissolution of carbonates are directly associated with poor and good qualities of deep reservoirs, respectively (Longstaffe et al., 2003; Mansurbeg et al., 2008; Morad et al., 2012; Wang et

al., 2016) However, the evolution of the paleo-fluid in the reservoir during burial and its influence on reservoir quality are rarely discussed. In the Dongying depression, various carbonate cements are widely distributed in reservoir rocks during diagenesis process, and the important authigenic minerals provide an effective media to investigate the fluid evolution. The carbon and oxygen isotopic compositions have been proved to be useful method to determine the cement characteristics and the fluid evolution (Liu et al., 2014; Mansurbeg et al., 2012; Wang et al., 2016). The oxygen isotopic are confined by the temperature, fractionation factor, and the source of fluids (Melezhik et al., 2003; Morad et al., 1990; Spezzaferri et al., 2002). In addition, the fluid inclusions could print the temperature of the paleo-fluid. $\delta^{13}C$ can trace the carbon origins during water-rock interaction process (Bourque et al., 2001; Liu et al., 2014; Sanyal et al., 2005; Yang et al., 2010).

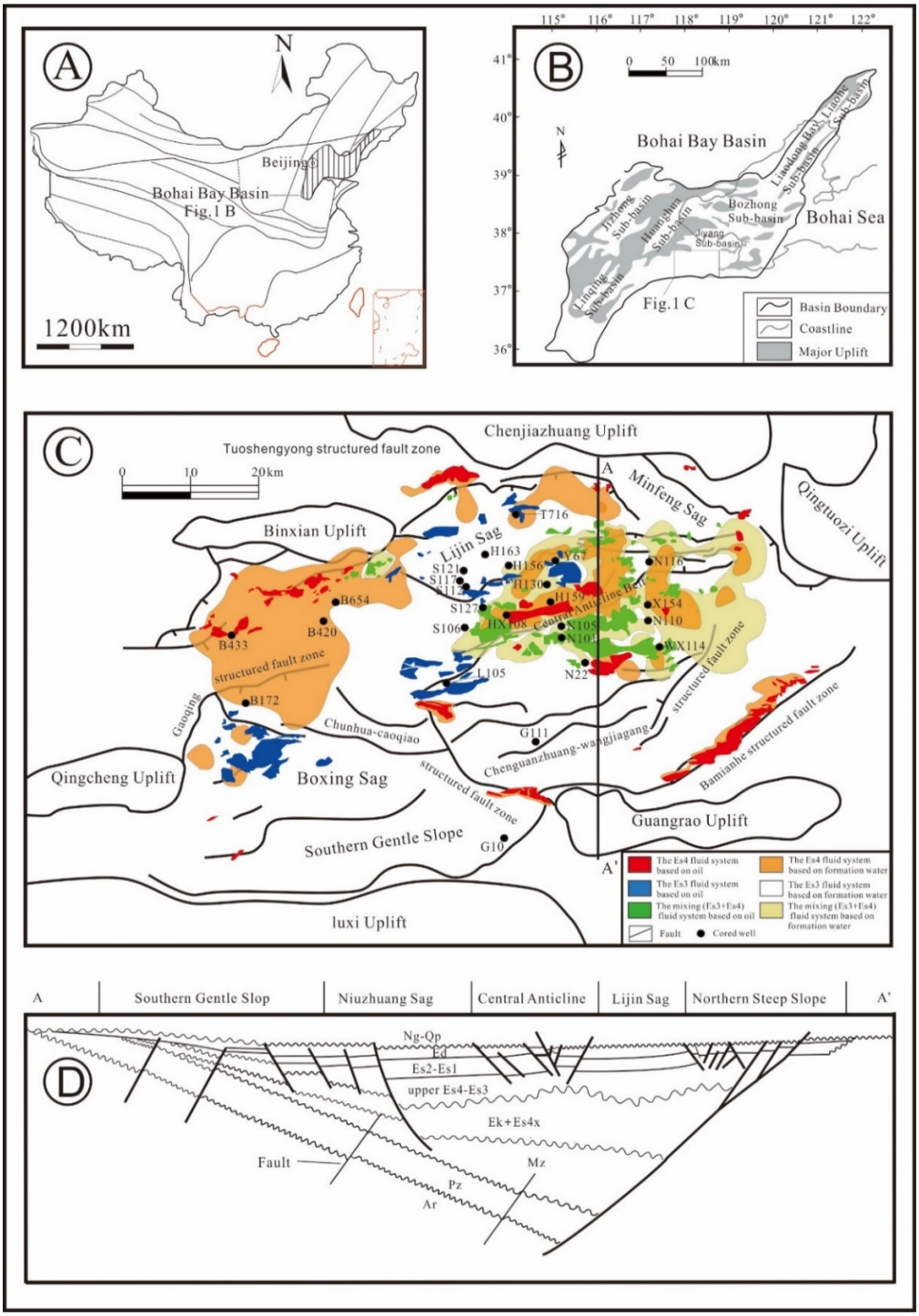

Figure 1. Geological map presenting the sampled wells location and the major tectonic units of the Dongying Depression (modified after Meng et al., 2018; Tian et al., 2017).

Hence, in this contribution, we focus on the diagenetic cements of the Es3, with the aim of characterizing typical cementation systems of sandstone reservoirs. We use the petrology studies, fluid inclusion, and stable isotope data to infer the interactions among fluid and rock during reservoir formation. Our results show that the $\delta^{13}C$ and $\delta^{18}O$ of Group II carbonate cements are more negative than those that belongs to Group I. Negative $\delta^{13}C$ values may record petroleum migration, and the difference in $\delta^{13}C$ and $\delta^{18}O$ between the two generations of carbonate cement may be used to determine the source of the fluid. Our results also highlight the importance of cementation system reworking for secondary pore reservoirs in sandstone units, and may improve future reservoir identification in the Dongying depression.

2. REGIONAL GEOLOGY

The Bohai Bay Basin is one of the most vital petroleum-rich basins in China, and it was formed as a Cenozoic rift (Fig. 1D). The petroliferous Jiyang sub-basin is situated within the south of the Bohai Bay basin and comprises four depressions: the Dongying, Huimin, Zhanhua, and Chezhen depressions, and a number of uplifted blocks (Fig. 1B–D). The Dongying Depression is situated in the southeastern part of Jiyang sub-basin, and underwent two tectonic events: a syn-rift stage and a post-rift stage, during the Paleogene (65.0–24.6 Ma) and from the Neogene to the present (24.6–0 Ma), respectively (Allen et al., 1997; Hsiao et al., 2010; Hu et al., 2001; Huang & Pearson, 1999; Qi, 2004; Xia et al., 2018). The Paleogene units comprise the Kongdian (Ek, 65.0–50.4 Ma), Shahejie (Es, 50.4–32.8 Ma), and Dongying (Ed, 32.8–24.6 Ma) formations from bottom to top. Neogene sections include the Guantao (Ng, 24.6–5.1 Ma), Minghuazhen (Nm, 5.1–2.0 Ma), and Pingyuan (Qp, 2–0 Ma) formations from bottom to top. Quaternary units are represented by the Pingyuan (Qp) Formation (Hao et al., 2011) (Fig. 2).

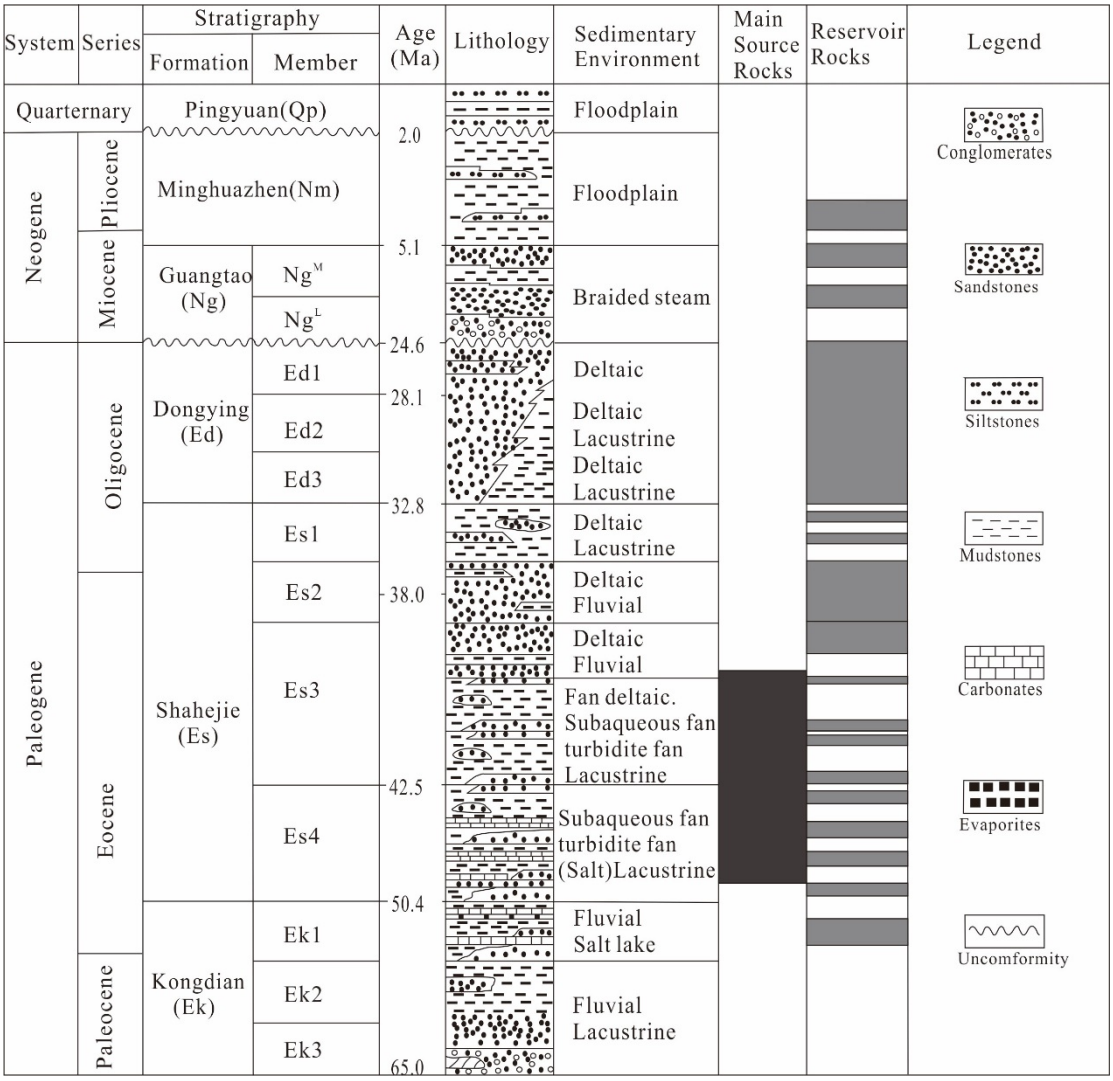

Figure 2. Cenozoic stratigraphy and lithological characteristics of the Dongying Depression (modified after Meng et al., 2018).

The Es3 (42–38 Ma) and Es4 (50.4–42 Ma) are the two major source rocks in the region (Hao et al., 2011; Tian et al., 2017).

The source rocks Es3 are dominated by lacustrine oil shales, mudstones, and calcareous mudstones that were deposited in semi-deep to deep lacustrine environments (Yuan et al., 2017). Es4 source rocks are gray mudstones, and the mudstones commonly consist of gypsum and halite interlayers, thus are inferred to have been formed in a salt-lake environment (Zhu et al., 2004). The difference in depositional environment between Es4 and Es3 has been used to determine fluid systems based on oil and formation water compositions (Qian & Zeng, 2009; Zhang et al., 2003; Zhu & Jin, 2003) (Fig. 1C). The upper part of Es3 is one of the most significant reservoirs in the region, and mainly consisting of deltaic sandstones (Hao et al., 2009b) (Fig. 2).

3. METHODOLOGY

Samples analyzed in this study were selected from drill cores from 30 wells in the Dongying Depression, and doubly polished to 0.03-mm-thick sections for the study of mineralogy and diagenesis. The drill core samples were collected by the routine core procedure. Porosity data from core plug analysis was conducted using routine porosimeter, which uses helium for measurements at Shengli oilfield company of China Petroleum & Chemical Corporation. Thin sections were stained by Alizarin Red S to aid with carbonate mineral identification. Diagenetic features, detrital grain composition, cement content, and surface pore structures were analyzed with a Leica 4500P polarizing microscope. Unidentifiable diagenetic minerals were further examined by cathodoluminescence (CL) imaging and scanning electron microscope (SEM).

Microthermometric measurements were conducted by a Linkam THMSG600 heating–freezing stage following standard procedures, in the fluid-inclusion laboratory at the State Key Laboratory of Petroleum Resources and Prospecting, China University of Petroleum, Beijing, China. The stage was calibrated at −56.6°C, −10.7°C, and 0.0°C using synthetic fluid inclusions (Fluid Inc.). The precision of measurements was estimated as ±0.2°C for < 30°C, and ±1°C for between 30°C and 200°C. Homogenization temperatures (Th) and freezing points (Tm, ice) of fluid inclusions were measured. We used a rate of 1−5°C/min during the initial stages of heating, which was reduced to 0.3−1°C/min when approaching the temperature of phase changes. Salinities of aqueous-fluid inclusions were calculated using the freezing point of H_2O–NaCl (Bodnar, 1993).

Carbon and oxygen isotopic compositions ($\delta^{13}C$ and $\delta^{18}O$) were determined at the State Key Laboratory of Petroleum Resources and Prospecting, China University of Petroleum, Beijing, China by gas isotope ratio mass spectrometry. The samples were crushed to 200 mesh, then allowed to react with the phosphoric acid for 1 hour in a water-bath thermostatic chamber at 25°C, and CO_2 gas was extracted following (Al-Aasm et al., 1990). Carbon and oxygen isotopes were measured using a MAT-253 mass spectrometer. All $\delta^{13}C$ and δ18O values are reported relative to the Pee Dee Belemnite standard (PDB). Analytical uncertainty (1σ) was better than 0.10‰ for $\delta^{13}C$ and 0.15‰ for $\delta^{18}O$.

4. RESULTS

The characteristics of petrology and mineralogy, the observation and microthermometry analysis of fluid inclusions, and the data of stable isotopic compositions are summarized as following:

4.1. Petrographic characteristics

Optical microscope observation of thin sections indicates that the sandstone samples comprise 31.0%–56.6% quartz (mean = 40.4%), 24.0%–44.1% feldspar (mean = 30.8%), and 16.4%–36.9% rock fragments (mean = 23.0%) (Table 1). Based on sandstone classification scheme (Folk, 1980), most of samples plot in the fields of feldspathic litharenite and lithic arkose (Fig. 3). Detrital grains are fine- to medium-grained, angular to sub-rounded, and show point contacts (Fig. 4a). Lithic fragments are dominantly metamorphic and igneous in origin, and include quartzite, schist, granite, and carbonate fragments. Porosity ranges from 4.2% to 25.0% (Table 1). Low-porosity samples display calcite cementation (Fig. 4a, d, e, h) or contain kaolinite within pore throats, which formed through the dissolution of feldspar (Fig. 4b, c, f, g). In contrast, high-porosity samples have undergone cement dissolution (Fig. 4i–k) or lack kaolinite within their pores (Fig. 4l).

4.2. Calcite cement

Carbonate cement is widespread throughout the samples and comprises <21.7% of the rock volume (Table 1). Two groups of carbonates are identifiable by their occurrence and colors in CL images. Group I carbonate cement displays an annular structure, fills primary pores (Fig. 4a, e), and exhibits bright red luminescence in CL images (Fig. 4m). In addition,

Group I cement has been replaced by quartz overgrowths (Fig. 4n). Group II calcite cement displays a granular structure, contains larger crystals than Group I, and is not luminescent in CL images (Fig. 4o). Furthermore, Group II calcite cement is observed to replace quartz or feldspar and has undergone variable degrees of dolomitization (Fig. 4k, p).

4.3. Fluid inclusions

Carbonate cement is widely distributed in the Shahejie (Es) formation sandstone (Fig. 4). Petroleum and aqueous inclusions are observed at intersections among Group II calcite cement within fracture trails (Fig. 5) and quartz overgrowths.

Few inclusions are observed in Group I calcite, due to their small grain size and the grains are too dark to allow identification of fluid inclusions.

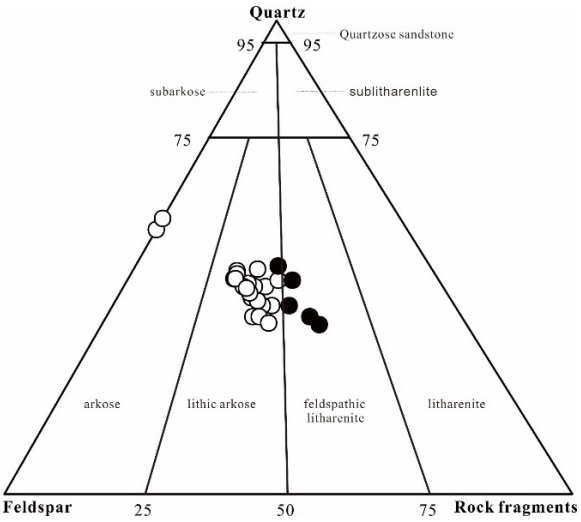

Figure 3. Composition of detrital clasts within the analyzed sandstone samples (based on Folk, 1980)

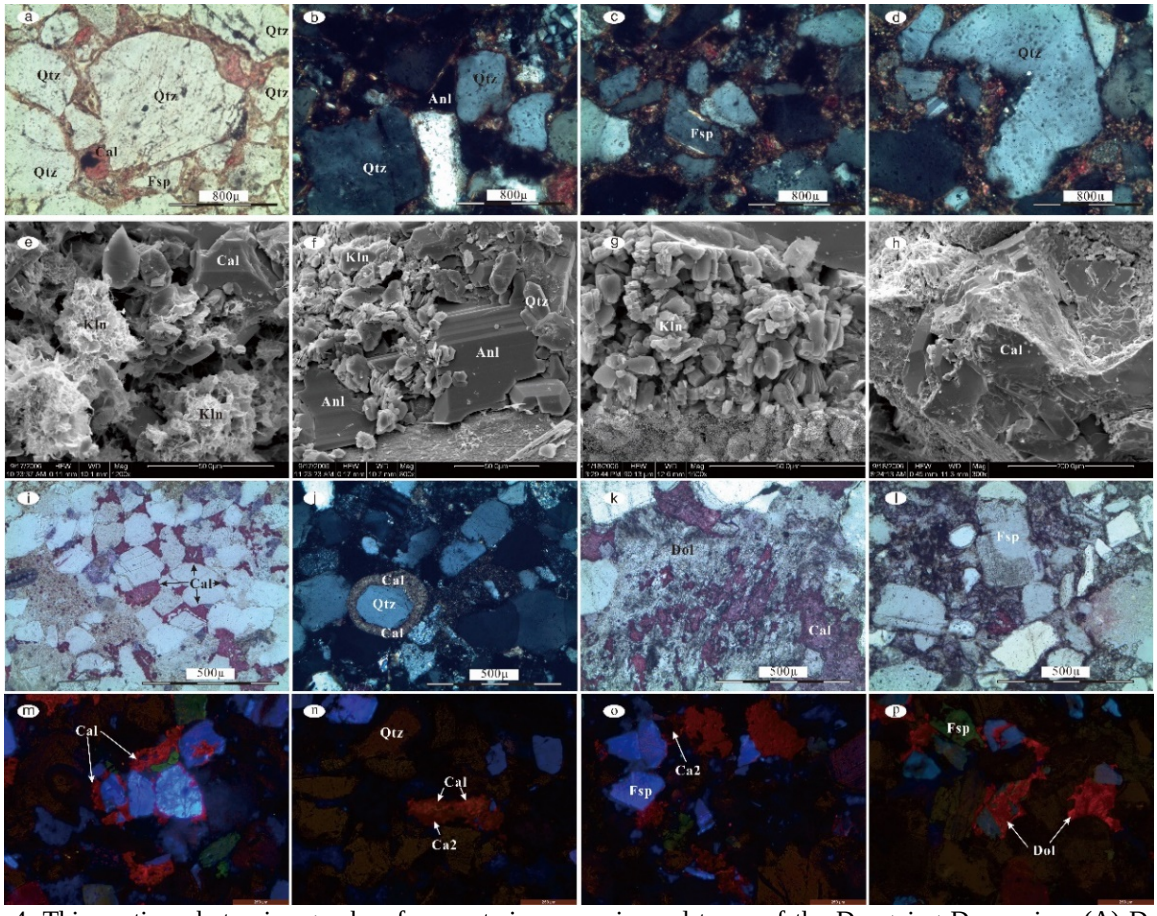

Figure 4. Thin-section photomicrographs of cements in reservoir sandstones of the Dongying Depression. (A) Detrital grains with point contacts and primary intergranular pores that are partially filled by microcrystalline calcite (Ca) observed in the well G111 at the 2104.25 m depth. (B) Pore throat partially filled by kaolinite, which replaced earlier analcime (Well G111, at 2115.49 m depth). (C) Pore throat partially filled with coexisting kaolinite and quartz overgrowths in well G111, 2104.25 m depth). (D) Calcite partially replacing a quartz grain in the well G111, observed at 2104.25 m depth. (E–H) SEM images of A–D. (i) Dissolution pores (DP) that were produced during dissolution of Ca1 and detrital grains, and were later filled by ferrocalcite in the Well N22, at 3208.78 m depth. (j) Calcite completely filling a circular pore observed in the well no. N22, 3228.91 m depth. (k) Dolomitization resulting from the dissolution of Ca1 and detrital grains (well no. N22, 3232.6 m depth. (l) Dissolution of a feldspar (Fsp) grain (N22 Well, 3231.1 m depth. (m-p) CL images of Ca1, Ca2, feldspar and quartz observed in the well N10, 3044.6-3099.1 m depth

Table 1. Diagenetic cements, porosity and stable isotopic compositions of carbonate cements in Es3 reservoirs in the Dongying Depression

Sample No.	Well	Depth (m)	Fm	Lithology	Grains (%)			Cements (%)					Porosity (%)	$\delta^{13}C_{PDB}$ (‰)	$\delta^{18}O_{PDB}$ (‰)
					Quartz	Feldspar	Rock fragments	Calcite	Dolomite	Quartz overgrowth	others % (minerals)	Group			
1	N105	3118.8	Es_3	medium lithic arkose	36.6	26.6	35.8	1.0	-	-	-	I	10.8	1.5	-14.2
2	N101	3050.5	Es_3	fine lithic arkose	31.0	24.8	21.7	0.8	19.4	0.8	1.6. (Kaolinite)	II	8.7	-1.1	-5.5
3	N110	3000.6	Es_3	very fine arkose	40.9	32.0	16.4	7.1	2.7	0.9	-	I	21.3	3.5	-12.0
4	N110	3004.8	Es_3	fine lithic arkose	33.2	28.2	22.0	12.4	1.7	0.8	1.7, (charcoal)	I	15.2	4.3	-12.3
5	S106	3398.7	Es_3	fine lithic arkose	40.4	28.4	22.9	5.5	1.8	0.5	0.5, (siderite)	I	16.2	3.3	-13.5
6	H130	2404.0	Es_3	fine arkose	46.8	34.1	18.0	-	1.0	-	-	I	22.9	5.0	-7.3
7	H130	2780.4	Es_3	medium arkose	38.6	31.4	20.6	-	9.0	0.4	-	I	15.2	2.7	-11.8
8	H163	2833.4	Es_3	fine-medium arkose	39.8	33.2	22.3	3.8	-	0.9	-	I	4.2	2.1	-10.6
9	L105	2767.1	Es_3	medium feldspathic litharenite	35.3	29.3	21.6	12.9	-	0.9	-	I	7.1	-2.5	-17.4
10	Y67	3068.7	Es_3	fine lithic arkose	38.6	24.0	22.7	7.7	3.4	0.4	0.4, 2.6, (siderite, Kaolinite)	I	13.5	2.9	-11.2
11	B654	2829.5	Es_3	fine-medium arkose	37.2	24.0	17.1	2.3	19.4	-	-	II	6.8	3.4	-4.9
12	H156	2752.8	Es_3	very fine arkose	43.5	32.9	22.7	-	1.0	-	-	II	15.4	-2.5	-8.9
13	H156	3215.5	Es_3	fine arkose	38.0	28.7	18.1	0.4	14.3	0.4	-	II	7.6	-4.3	-7.6
14	H159	2954.3	Es_3	fine lithic arkose	35.0	25.2	36.9	-	2.9	-	-	II	7.0	1.0	-5.1
15	HX108	3481.8	Es_3	fine arkose	43.0	34.8	20.9	-	0.8	0.5	-	II	10.6	-2.2	-11.7
16	N22	3226.5	Es_3	fine lithic arkose	33.8	32.0	24.0	0.4	8.9	0.4	0.4, Kaolinite	I	21.9	3.0	-9.8
17	S127	3214.5	Es_3	fine lithic arkose	34.7	32.9	27.7	1.9	1.9	0.9	-	I	9.8	2.8	-9.9
18	T716	3217.9	Es_3	medium feldspathic litharenite	35.7	34.7	24.4	4.7	-	0.5	-	I	7.2	0.9	-14.1
19	X154	2936.5	Es_3	fine feldspathic litharenite	44.2	25.0	28.4	-	0.5	1.0	0.5, 0.5, (siderite, barite)	II	21.3	2.6	-10.4
20	G111	1981.4	Es_3	fine arkose	41.1	33.5	22.0	-	1.0	-	0.5, 1.9, (pyrite, Kaolinite)	II	16.9	-7.4	-7.2
21	G10	913.8	Es_3	fine lithic arkose	55.0	44.1	-	-	0.9	-	-	II	25.0	-9.8	-9.0
22	N116	3099.7	Es_3	fine lithic arkose	46.0	25.7	24.3	0.7	-	0.5	2.9, (siderite)	I	7.0	2.2	-13.9
23	S112	3042.4	Es_3	fine arkose	56.6	40.3	-	2.5	-	0.6	-	I	22.3	1.6	-10.6
24	S117	3332.5	Es_3	very fine arkose	38.8	30.8	19.4	8.8	-	0.4	1.8, (siderite)	I	6.8	1.3	-13.9
25	S117	3392.1	Es_3	very fine arkose	43.4	34.0	17.9	3.8	0.9	-	-	I	5.6	1.4	-14.0
26	S121	3530.0	Es_3	very fine arkose	43.3	32.3	17.1	1.8	5.5	-	-	II	7.8	-2.5	-11.9
27	WX114	2676.1	Es_3	medium feldspathic litharenite	40.0	29.0	31.0	-	-	-	-		12.0	2.7	-7.3
28	B172	2828.5	Es_3	argillaceous limestone	-	-	-	-	-	-	-		-	2.5	-13.2
29	B420	2626.0	Es_3	argillaceous dolomite	-	-	-	-	-	-	-		-	3.3	-6.2
30	B433	1659.4	Es_3	dolomitic limestone	-	-	-	-	-	-	-		-	0.8	-12.9

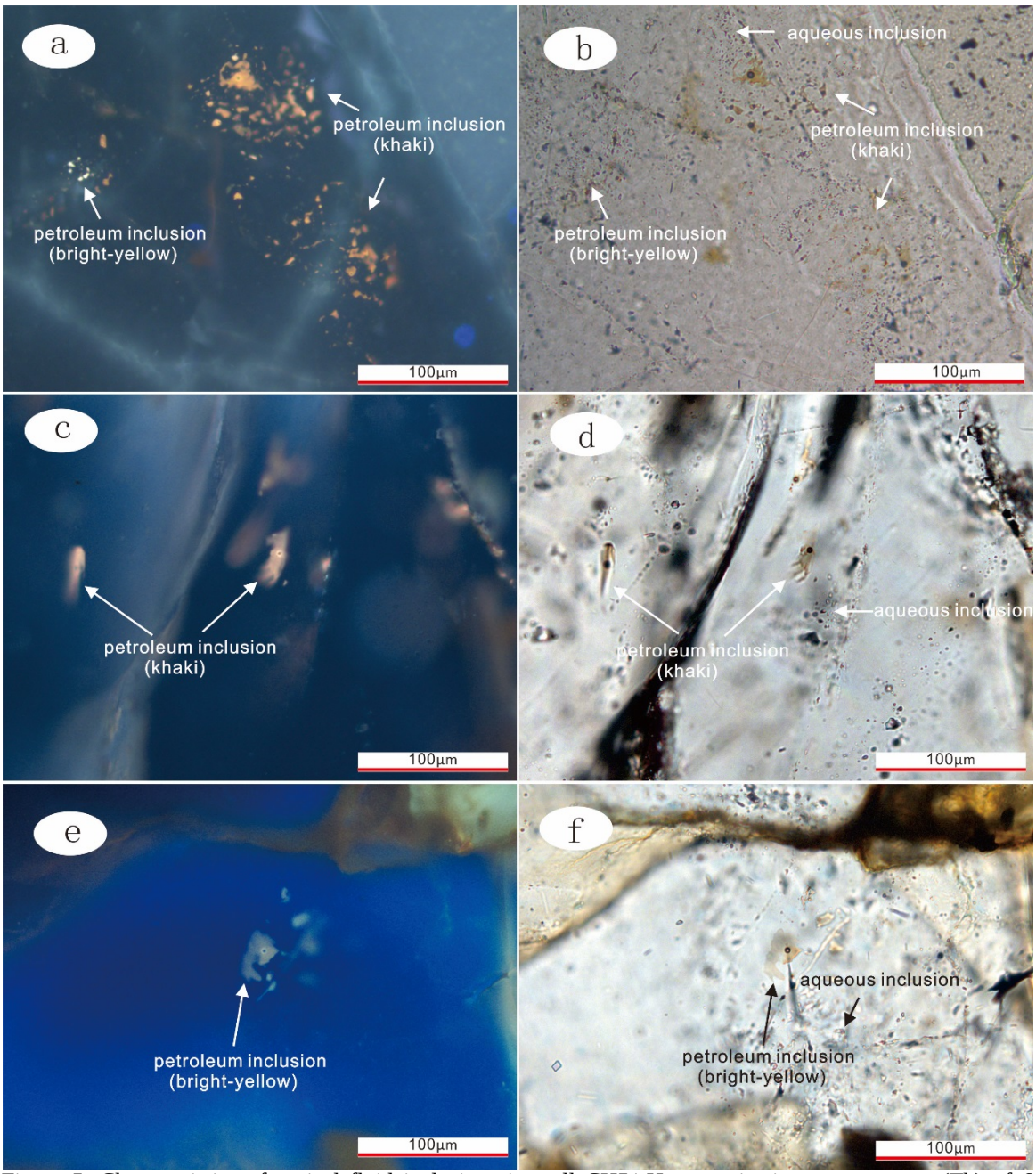

Figure 5. Characteristics of typical fluid inclusions in well CH51.Homogenization temperatures (Th) of 68 aqueous inclusions in calcite cements and quartz overgrowths from well CH51 (Table 2) were measured. Aqueous inclusions that were coeval with khaki-colored petroleum inclusions (type-I) have T_h values of 106°C to 126°C. Type-I aqueous inclusions yielded ice-melting temperatures ($T_{m,\,ice}$) of −2.5°C to −2.9°C (4.1 to 4.8 wt.% NaCl eqv.). Aqueous inclusions that are coeval with bright-yellow-colored oil inclusions (type-II) were homogenized to a liquid phase at temperatures between 83°C and 166°C, with a peak temperature of 100 – 130°C. Type-II inclusions yielded ice-melting temperatures ($T_{m,ice}$) of −0.3°C to −21.6°C (0.5 to 22.6 wt.% NaCl eqv.). The microthermometric data are summarized in Figures 6 and 7.

Three fluid-inclusion types are identified based on their UV-epifluorescence characteristics and their phases at room temperature (21°C): (1) petroleum inclusions that display a bright-yellow color under UV light; (2) petroleum inclusions with khaki color under UV light; and (3) aqueous inclusions that coexist with the two above-mentioned petroleum inclusions. We selected large inclusions with regular shapes for microthermometry analysis. Bright-yellow- and khaki-colored petroleum inclusions are observed in Group II calcite cements and quartz overgrowths, respectively. All aqueous inclusions contain two phases (L–V; Fig. 5) at room temperature (21°C), and most are ellipsoidal and ~15 μm in size. Aqueous inclusions are observed within calcite cements and quartz overgrowths, and are closely associated with petroleum inclusions.

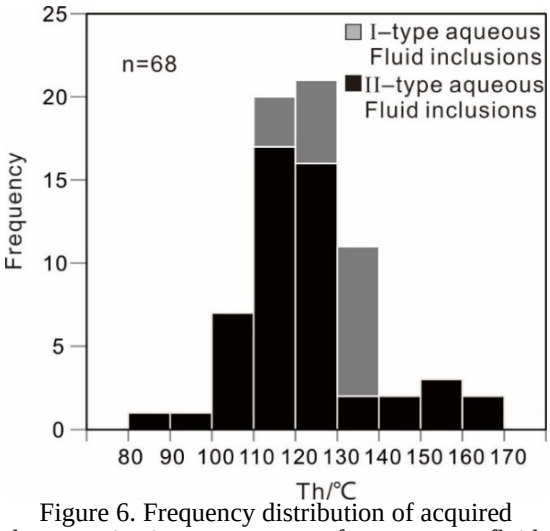

Figure 6. Frequency distribution of acquired homogenization temperatures from aqueous fluid inclusions.

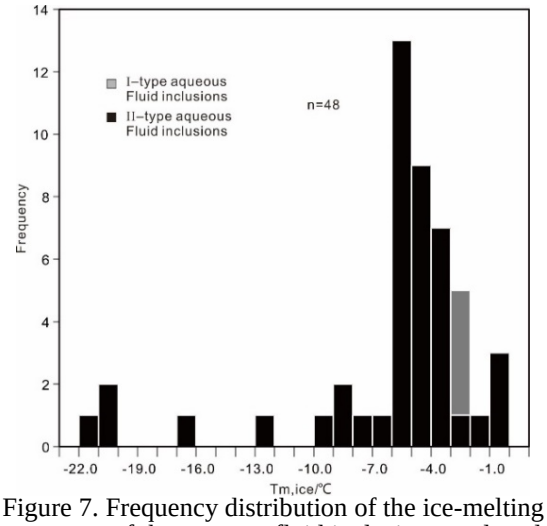

Figure 7. Frequency distribution of the ice-melting temperature of the aqueous fluid inclusions analyzed in this study

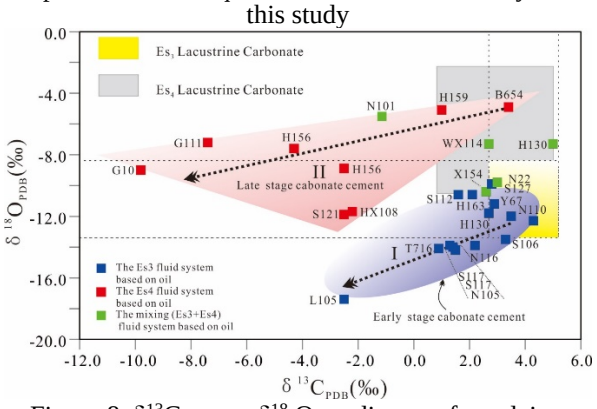

Figure 8. $\delta^{13}C_{PDB}$ vs. $\delta^{18}O_{PDB}$ diagram for calcite cements.

4.4. Carbon and oxygen isotopic compositions

Carbon and oxygen isotopic compositions of whole-rock samples were analysed to represent the isotopic compositions of the carbonate cements. The δ13C and δ18O values of the carbonate cements vary between –9.8‰ and 5.0‰, and –17.4‰ and –4.9‰, respectively (Table 1 and Fig. 8). As mentioned above (Section 4.2), two groups of carbonate cement are distinguished based on their petrologic characteristics. The isotopic compositions of the two cements are also distinct; i.e., Group I calcite-dominant cement yields more negative δ18O and heavier δ13C than Group II dolomite-dominant cement (Table 1).

5. DISCUSSION

5.1. Isotopic composition of paleo-lake water

Carbon within the analyzed cements was likely derived from organic matter and paleo-lake water. Organic matter is characterized by a highly negative carbon isotopic composition, typically between –35‰ and –20‰ (Dutton & Land, 1985; Irwin et al., 1977; Macaulay et al., 2000; Rosenbaum & Sheppard, 1986; Sullivan et al., 1990). In the Dongying Depression, paleo-lake water isotopic composition is constrained by carbonate interlayers in the lacustrine hydrocarbon source rocks of the Shahejie Formation. The $\delta^{13}C$ and $\delta^{18}O$ values of carbonates in the Es3 range from 2.7‰ to 5.2‰ and from –8.4‰ to –13.4‰, respectively (Liu, 2017) (Fig. 8). The $\delta^{13}C$ and $\delta^{18}O$ values of carbonates in the Es4 range from 3.0‰ to 5.4‰ and from –8.6‰ to –4.2‰, respectively (Cai et al., 2009; Liu, 2017) (Fig. 8). The $\delta^{13}C$ compositions of carbonates from Es3 and Es4 are similar; however, the carbonates in Es4 yield a heavier $\delta^{18}O$ isotopic composition than those in Es3. To explain these results, we propose that during the deposition of Es4, the volume of lake water decreased, resulting in the widespread evaporation and fractionation of oxygen isotope, thereby producing heavier $\delta^{18}O$ values (Cai et al., 2009).

5.2. Origin of calcite cements

We divide the analyzed calcite cements into two groups based on their isotopic compositions (Fig. 8). It suggests that the Group I cements are dominated by fluid derived from Es3, and yield lower values of δ13C and δ18O (–2.5‰ to 5.0‰ and –17.4‰ to -7.3‰, respectively) than values of the lacustrine carbonate in Es3.

Group II cements formed in the Es4 system, and yield lower $\delta^{13}C$ and $\delta^{18}O$ (–9.8‰ to 3.4‰ and –11.9‰ to -4.9‰, respectively) than Es4 lacustrine carbonate. Furthermore, the $\delta^{18}O$ values of Group II cements are heavier than those of Group I cements (Table 1, Fig. 8).

Table 2. Microthermometric data of the CH51 well fluid inclusions.

Sample	Th	Tm,ice	Salinity	type	Coexisting inclusions
CH51-1	121	-	-	2-phase L-V Aq FIs	khaki-colored petroleum inclusions
CH51-1	114	-8.5	12.2	2-phase L-V Aq FIs	yellow-colored petroleum inclusions
CH51-1	116	-5.0	7.8	2-phase L-V Aq FIs	yellow-colored petroleum inclusions
CH51-1	119	-9.1	12.9	2-phase L-V Aq FIs	yellow-colored petroleum inclusions
CH51-1	122	-8.6	12.3	2-phase L-V Aq FIs	yellow-colored petroleum inclusions
CH51-1	115	-5.5	8.5	2-phase L-V Aq FIs	yellow-colored petroleum inclusions
CH51-2	124	-3.2	5.2	2-phase L-V Aq FIs	yellow-colored petroleum inclusions
CH51-2	123	-0.9	1.6	2-phase L-V Aq FIs	yellow-colored petroleum inclusions
CH51-2	121	-3.7	6.0	2-phase L-V Aq FIs	yellow-colored petroleum inclusions
CH51-2	121	-3.9	6.3	2-phase L-V Aq FIs	yellow-colored petroleum inclusions
CH51-2	110	-3.7	6.0	2-phase L-V Aq FIs	yellow-colored petroleum inclusions
CH51-2	108	-3.0	4.9	2-phase L-V Aq FIs	yellow-colored petroleum inclusions
CH51-2	114	-5.1	8.0	2-phase L-V Aq FIs	yellow-colored petroleum inclusions
CH51-2	115	-2.8	4.6	2-phase L-V Aq FIs	khaki-colored petroleum inclusions
CH51-2	110	-5.5	8.5	2-phase L-V Aq FIs	yellow-colored petroleum inclusions
CH51-2	113	-1.8	3.0	2-phase L-V Aq FIs	yellow-colored petroleum inclusions
CH51-3	115	-5.9	9.0	2-phase L-V Aq FIs	yellow-colored petroleum inclusions
CH51-3	119	-5.4	8.4	2-phase L-V Aq FIs	yellow-colored petroleum inclusions
CH51-3	114	-4.8	7.5	2-phase L-V Aq FIs	yellow-colored petroleum inclusions
CH51-3	106	-	-	2-phase L-V Aq FIs	khaki-colored petroleum inclusions
CH51-3	104	-0.3	0.5	2-phase L-V Aq FIs	yellow-colored petroleum inclusions
CH51-3	97	-0.7	1.2	2-phase L-V Aq FIs	yellow-colored petroleum inclusions
CH51-3	127	-2.1	3.5	2-phase L-V Aq FIs	yellow-colored petroleum inclusions
CH51-3	112	-	-	2-phase L-V Aq FIs	khaki-colored petroleum inclusions
CH51-3	110	-	-	2-phase L-V Aq FIs	khaki-colored petroleum inclusions
CH51-3	107	-4.4	7.0	2-phase L-V Aq FIs	yellow-colored petroleum inclusions
CH51-3	119	-4.8	7.5	2-phase L-V Aq FIs	yellow-colored petroleum inclusions
CH51-3	122	-5.4	8.4	2-phase L-V Aq FIs	yellow-colored petroleum inclusions
CH51-3	108	-4.8	7.5	2-phase L-V Aq FIs	yellow-colored petroleum inclusions
CH51-3	103	-5.9	9.0	2-phase L-V Aq FIs	yellow-colored petroleum inclusions
CH51-4	164	-	-	2-phase L-V Aq FIs	yellow-colored petroleum inclusions
CH51-4	159	-	-	2-phase L-V Aq FIs	yellow-colored petroleum inclusions
CH51-4	149	-	-	2-phase L-V Aq FIs	yellow-colored petroleum inclusions
CH51-4	129	-	-	2-phase L-V Aq FIs	yellow-colored petroleum inclusions
CH51-4	143	-	-	2-phase L-V Aq FIs	yellow-colored petroleum inclusions
CH51-4	136	-	-	2-phase L-V Aq FIs	yellow-colored petroleum inclusions
CH51-4	83	-	-	2-phase L-V Aq FIs	yellow-colored petroleum inclusions
CH51-4	123	-3.1	5.1	2-phase L-V Aq FIs	yellow-colored petroleum inclusions
CH51-4	126	-	-	2-phase L-V Aq FIs	khaki-colored petroleum inclusions
CH51-4	125	-	-	2-phase L-V Aq FIs	khaki-colored petroleum inclusions
CH51-4	120	-	-	2-phase L-V Aq FIs	khaki-colored petroleum inclusions
CH51-4	129	-4.7	7.4	2-phase L-V Aq FIs	yellow-colored petroleum inclusions
CH51-4	134	-5.7	8.8	2-phase L-V Aq FIs	yellow-colored petroleum inclusions
CH51-4	117	-21.6	22.6	2-phase L-V Aq FIs	yellow-colored petroleum inclusions
CH51-4	116	-20.7	22.1	2-phase L-V Aq FIs	yellow-colored petroleum inclusions
CH51-4	117	-20.5	22.0	2-phase L-V Aq FIs	yellow-colored petroleum inclusions
CH51-5	118	-5.4	8.4	2-phase L-V Aq FIs	yellow-colored petroleum inclusions
CH51-5	120	-3.6	5.8	2-phase L-V Aq FIs	yellow-colored petroleum inclusions
CH51-5	123	-5.9	9.0	2-phase L-V Aq FIs	yellow-colored petroleum inclusions
CH51-5	125	-5.4	8.4	2-phase L-V Aq FIs	yellow-colored petroleum inclusions
CH51-5	123	-2.9	4.8	2-phase L-V Aq FIs	khaki-colored petroleum inclusions
CH51-5	120	-6.5	9.8	2-phase L-V Aq FIs	yellow-colored petroleum inclusions
CH51-5	125	-	-	2-phase L-V Aq FIs	khaki-colored petroleum inclusions
CH51-5	129	-4.1	6.6	2-phase L-V Aq FIs	yellow-colored petroleum inclusions
CH51-5	125	-	-	2-phase L-V Aq FIs	khaki-colored petroleum inclusions
CH51-5	128	-4.2	6.7	2-phase L-V Aq FIs	yellow-colored petroleum inclusions
CH51-5	121	-5.8	8.9	2-phase L-V Aq FIs	yellow-colored petroleum inclusions
CH51-5	126	-	-	2-phase L-V Aq FIs	khaki-colored petroleum inclusions
CH51-5	116	-4.0	6.4	2-phase L-V Aq FIs	yellow-colored petroleum inclusions
CH51-5	123	-4.1	6.6	2-phase L-V Aq FIs	yellow-colored petroleum inclusions
CH51-5	119	-	-	2-phase L-V Aq FIs	khaki-colored petroleum inclusions
CH51-5	160	-16.0	19.2	2-phase L-V Aq FIs	yellow-colored petroleum inclusions
CH51-5	159	-12.0	15.9	2-phase L-V Aq FIs	yellow-colored petroleum inclusions
CH51-5	166	-7.2	10.7	2-phase L-V Aq FIs	yellow-colored petroleum inclusions
CH51-5	120	-	-	2-phase L-V Aq FIs	khaki-colored petroleum inclusions
CH51-5	121	-2.9	4.8	2-phase L-V Aq FIs	khaki-colored petroleum inclusions
CH51-5	126	-	-	2-phase L-V Aq FIs	khaki-colored petroleum inclusions
CH51-5	106	-2.5	4.1	2-phase L-V Aq FIs	khaki-colored petroleum inclusions

The isotopic compositions of Group I samples reflect changes in environment relative to Es3 lacustrine carbonate. The negative $\delta^{13}C$ values of Group I samples likely resulted from an increase in organic carbon content due to thermal degradation of Es3 source rocks. The large variation in $\delta^{13}C$ values (–2.5‰ to 5.0‰) suggests a variable degree of mixing between organic and inorganic carbon (Fig. 8). Such mixing processes would also influence $\delta^{18}O$, because fluid derived from deep source rocks typically has a more negative $\delta^{18}O$ value than lake water (Lawrence et al., 1975; Perry et al., 1976). The high $\delta^{18}O$ values of Group II samples indicate that the precipitating fluids were more enriched in ^{18}O than Es3 paleo-lake water. Given that (1) calcite cements derived from Es4 yield higher $\delta^{18}O$ values than Es3, and (2) $\delta^{18}O$ values decrease with depth, we infer that $\delta^{18}O$ values in Group II cements reflect mixing between fluids derived from Es3 and Es4. The high $\delta^{18}O$ values reported for Group II cements likely resulted from interaction with Es4 source rocks, which formed in an evaporation environment. This conclusion is consistent with oil-source comparison studies that indicate wells within the Es3 fluid system (Fig. 1C) contain calcite-dominated with C and O isotopic compositions of Group I. In contrast, wells in the Es4 fluid system (Fig. 1C) contain dolomite-dominated cements and have C and O isotopic compositions of Group II (Fig. 8).

5.3. Evolution of paleo-fluids

We infer that, following deposition, Es3 was subjected to alternating cycles of acidic and alkaline diagenetic environments. At shallow depths, sedimentary environments are typically alkaline, with diagenetic products represented by early calcite. With the progressive buried of the deposits, fluids evolved to more acidic compositions, resulting in dissolution of feldspar and the development of quartz overgrowths that replaced early calcite. Early calcite in our samples is fine-grained and opaque, which prevents the identification of fluid inclusions. Instead, we conducted microthermometry analysis on aqueous fluid inclusions within quartz overgrowths. Homogenization temperatures range from 106°C to 126°C, and salinity varies from 4.1 to 4.8 wt.% NaCl eqv. Due to the early calcite is formed before quartz overgrowth, the formation temperature of early calcite is no more than 106°C. Furthermore, we calculated the O isotopic compositions of early stage fluid based on isotope fractionation factor of calcite and water (Zheng & Chen, 2000) and formation temperature (106°C). The $\delta^{18}O$ values of early stage fluid vary from –34.7‰ to -24.6‰, which fall into the range of meteoric waters (Hoefs, 2009). It suggests that the early stage fluid is dominated by shallow fluid system.

As the sediments were buried deeper, organic acids were gradually consumed and the depositional environment interstitial fluid became more alkaline. During this process, montmorillonite was converted to illite, and the iron content in newly formed carbonate minerals increased. Hence, late-stage calcite cement (Ca2) does not display luminescent in CL images. Aqueous fluid inclusions in late dolomite yield higher homogenization temperatures (up to 166°C) and salinities (up to 22.6 wt.% NaCl eqv.). Based on the isotope fractionation factor of dolomite and water (Hoefs, 2009) and the peak temperature of fluid inclusions in late dolomite (120°C), the $\delta^{18}O$ values of late stage fluid vary from -28.5‰ to -21.5‰. The heavier $\delta^{18}O$ values are likely indicating fluid input from a deep source.

A further stage of diagenesis is recorded by the dissolution of late-stage carbonate cements, indicating a transition back to an acidic fluid composition. We speculate that this change in fluid properties may represent a renewal of the hydrocarbon generation process in the source rocks.

5.4. Impact on reservoir quality and petroleum accumulation

Carbonate cements play a key role in controlling reservoir quality, which in turn influences hydrocarbon accumulation (Esteban & Taberner, 2003; Heasley et al., 2000; Neilson & Oxtoby, 2008). As show in Figure 9, Group I calcite cement, derived from paleo-lake water, reduced the porosity of the sandstone during diagenesis (Fig. 4a, d). The carbon isotope values of calcite cement are more negative, the porosity of the reservoir becomes smaller. During this process, acidic fluid containing carbon dioxide and carboxylic acid flowed into the reservoir rocks, resulting in the dissolution of feldspar and generation of kaolinite (Fig. 4b–c). This kaolinite may also have contributed to filling pore-space (Wang et al., 2016), and aluminosilicate minerals may have acted as a pH buffer, which would reduce the ability of carboxylic acid to dissolve calcite (Seewald, 2003).

However, late-stage carbonate cements show distinct organic acid contributions and contain abundant secondary pores. The porosity of reservoir becomes larger (6.8% ~ 25%) as the carbon isotope becomes more negative (3.4‰ ~ -9.8‰) except the

Sample No.19. (Table 1, Fig. 9). The more and more organic acids were generated by thermo-catalytic degradation of kerogen and produced negative $\delta^{13}C$ values in late-stage carbonate cements. The multiple acidic fluid charging which greatly improved the ability of organic acids to dissolve and erode pores in the deep reservoir.

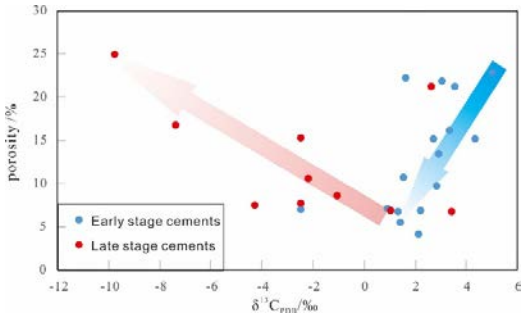

Figure 9. $\delta^{13}C_{PDB}$ vs. porosity diagram for calcite cements.

6. CONCLUSIONS

The main conclusions are the next:

(1) In the Es3 sandstone reservoirs of the Dongying Depression, we observed abundant secondary pores that are related to the reworking of the cementation system. The production of such pores allowed for subsequent petroleum accumulation.

(2) The presence of ^{13}C-depleted calcite cement (relative to lacustrine carbonate) is potentially a trace of hydrocarbon migration. Furthermore, differences in C–O isotopic compositions may be used to distinguish between Es3 and Es4 fluid sources in our research region.

Although our study is focused on the Dongying Depression, Bohai Bay Basin, China, our results could be applied to any sedimentary basin where considerable carbonate cements in clastic sedimentary rock reservoirs exist. This work has potentially wider implications in petroleum exploration, such as indicator of hydrocarbon migration and difference fluid sources.

Acknowledgements

This work was supported by National Science and Technology Major Project, China (No. 2016ZX05006-001). The authors are also grateful to Shengli Oilfield Company of Sinopec for assistance during the field trip and providing original geological data.

REFERENCES

Al-Aasm, I. S., Taylor, B. & South, B. 1990. *Stable isotope analysis of multiple carbonate samples using selective acid extraction.* Chemical Geology, 80, 119-125.

Allen, M. B., Macdonald, D. I. M., Zhao, X., Vincent, S. J. & Brouet-Menzies, C. 1997. *Early Cenozoic two-phase extension and late Cenozoic thermal subsidence and inversion of the Bohai Basin, northern China.* Marine and Petroleum Geology, 14: 951-972.

Bodnar, R. J. 1993. *Revised equation and stable for determining the freezing point depression of H_2O-NaCl solutions.* Geochimica et Cosmochimica Acta, 57: 683-684.

Bourque, P. A., Savard, M. M., Chi, G. X. & Dansereau, P. 2001. *Diagenesis and porosity evolution of the Upper Silurian-lowermost Devonian West Point reef limestone, eastern Gaspe Belt, Quebec Appalachians.* Bulletin of Canadian Petroleum Geology, 49: 299-326.

Cai, G. Q., Guo, F., Liu, X. T. & Sui, S. L. 2009, *Carbon and oxygen isotope characteristics and Palaeoenvironmental implications of lacustrine carbonate rocks from the Shahejie Formation in the Dongying sag.* Earth and Environment, 37: 347-354.

Dutton, S. P. & Land, L. S. 1985, *Meteoric burial diagenesis of Pennsylvanian arkosic sandstones, southwestern Anadarko Basin, Texas.* AAPG Bulletin, 69: 22-38.

Esteban, M. & Taberner, C. 2003, *Secondary porosity development during late burial in carbonate reservoirs as a result of mixing and/or cooling of brines:* Journal of Geochemical Exploration, 78: 355-359.

Folk, R. L. 1980, *Petrology of sedimentary rocks.* Hemphill Publishing Company, Austin, United States.

Hao, F., Zhou, X. H., Zhu, Y. M., Bao, X. H. & Yang, Y. Y. 2009a, *Charging of the Neogene Penglai 19-3 field, Bohai Bay Basin, China: Oil accumulation in a young trap in an active fault zone.* AAPG bulletin, 93: 155-179.

Hao, F., Zhou, X. H., Zhu, Y. M, Zou, H. Y., Bao, X. H. & Kong, Q. Y. 2009b, *Mechanisms of petroleum accumulation in the Bozhong sub-basin, Bohai Bay Basin, China. Part 1: Origin and occurrence of crude oils.* Marine and Petroleum Geology, 26: 1528-1542.

Hao, F., Zhou, X. H., Zhu, Y. M. & Yang, Y. Y. 2011, *Lacustrine source rock deposition in response to co-evolution of environments and organisms controlled by tectonic subsidence and climate, Bohai Bay Basin, China.* Organic Geochemistry, 42: 323-339.

Heasley, E. C., Worden, R. H. & Hendry, J. P. 2000, *Cement distribution in a carbonate reservoir: recognition of a palaeo oil–water contact and its relationship to reservoir quality in the Humbly Grove field, onshore, UK.* Marine and Petroleum Geology, 17: 639-654.

Hoefs, J. 2009. *Stable Isotope Geochemistry.* Springer-Verlag, Berlin Heidelberg, Germany.

Hsiao, L. Y., Graham, S. & Tilander, N. 2010. *Stratigraphy and sedimentation in a rift basin modified by synchronous strike-slip deformation: southern Xialiao basin, Bohai, offshore China.* Basin Research, 22: 61-78.

Hu, S. B., O'Sullivan, P. B., Raza, A. & Kohn, B. P. 2001. *Thermal history and tectonic subsidence of the Bohai Basin, northern China: a Cenozoic rifted and local pull-apart basin.* Physics of the Earth and Planetary Interiors, 126: 221-235.

Huang, H. P. & Pearson, M. J. 1999. *Source rock palaeoenvironments and controls on the distribution of dibenzothiophenes in lacustrine crude oils, Bohai Bay Basin, eastern China.* Organic Geochemistry, 30: 1455-1470.

Irwin, H., Curtis, C. & Coleman, M. 1977. *Isotopic evidence for source of diagenetic carbonates formed during burial of organic-rich sediments.* Nature, 269: 209-213.

Lawrence, J., Gieskes, J. & Broecker, W. 1975. *Oxygen isotope and cation composition of DSDP pore waters and the alteration of Layer II basalts.* Earth and Planetary Science Letters, 27: 1-10.

Liu, Q. 2017. *Composition and geological significance of carbon and oxygen isotopes in hydrocarbon source rocks , Dongying Sag , Bohai Bay Basin.* Petroleum Geology & Experiment, 39: 6.

Liu, S. B., Huang, S. J., Shen, Z. M., Lu, Z. X. & Song, R. C. 2014. *Diagenetic fluid evolution and water-rock interaction model of carbonate cements in sandstone: An example from the reservoir sandstone of the Fourth Member of the Xujiahe Formation of the Xiaoquan-Fenggu area, Sichuan Province, China.* Science China-Earth Sciences, 57: 1077-1092.

Longstaffe, F. J., Calvo, R., Ayalon, A. & Donaldson, S. 2003, *Stable isotope evidence for multiple fluid regimes during carbonate cementation of the Upper Tertiary Hazeva Formation, Dead Sea Graben, southern Israel.* Journal of Geochemical Exploration, 80: 151-170.

Macaulay, C., Fallick, A., Haszeldine, R. & McAulay, G. 2000, *Oil migration makes the difference: regional distribution of carbonate cement $\delta^{13}C$ in northern North Sea Tertiary sandstones.* Clay Minerals, 35: 69-69.

Mansurbeg, H., Morad, S., Salem, A., Marfil, R., El-ghali, M. A. K., Nystuen, J. P., Caja, M. A., Amorosi, A., Garcia, D. & La Iglesia, A. 2008, *Diagenesis and reservoir quality evolution of palaeocene deep-water, marine sandstones, the Shetland-Faroes Basin, British continental shelf.* Marine and Petroleum Geology, 25: 514-543.

Mansurbeg, H., De Ros, L. F., Morad, S., Ketzer, J. M., El-Ghali, M. A. K., Caja, M. A. & Othman, R. 2012, *Meteoric-water diagenesis in late Cretaceous canyon-fill turbidite reservoirs from the Espirito Santo Basin, eastern Brazil.* Marine And Petroleum Geology, 37: 7-26.

Melezhik, V. A., Fallick, A. E., Smirnov, Y. P. & Yakovlev, Y. N. 2003, *Fractionation of carbon and oxygen isotopes in C-13-rich Palaeoproterozoic dolostones in the transition from medium-grade to high-grade greenschist facies: a case study from the Kola Superdeep Drillhole.* Journal of the Geological Society, 160: 71-82.

Meng, W., Zeng, J. H., Cao, Z., Song, G. Q., Wang, Y. S., Teng, J. L. & Guo, Z. J. 2018, *Material Exchange and Migration between Pore Fluids and Sandstones during Diagenetic Processes in Rift Basins: A Case Study Based on Analysis of Diagenetic Products in Dongying Sag, Bohai Bay Basin, East China*. Geofluids.

Morad, S., Al-Aasm, I. S., Ramseyer, K., Marfil, R. & Aldahan, A. A. 1990. *Diagenesis of carbonate cements in Permo-Triassic sandstones from the Iberian Range, Spain: evidence from chemical composition and stable isotopes.* Sedimentary Geology, 67: 281-295.

Morad, S., Al-Aasm, I. S., Nader, F. H., Ceriani, A., Gasparrini, M. & Mansurbeg, H. 2012. *Impact of diagenesis on the spatial and temporal distribution of reservoir quality in the Jurassic Arab D and C members, offshore Abu Dhabi oilfield, United Arab Emirates.* Geoarabia, 17: 17-56.

Neilson, J. & Oxtoby, N. 2008. *The relationship between petroleum, exotic cements and reservoir quality in carbonates–A review.* Marine and Petroleum Geology, 25: 778-790.

Perry, E. A., Gieskes, J. & Lawrence, J. 1976. *Mg, Ca and O^{18}/O^{16} exchange in the sediment-pore water system, hole 149, DSDP.* Geochimica et Cosmochimica Acta, 40: 413-423.

Qi, J. F. 2004. *Two tectonic systems in the Cenozoic Bohai Bay basin and their genetic interpretation.* Chinese Geology, 31: 15-22.

Qian, S. Y. & Zeng, J. H. 2009. *Chemical characteristics of Shahejie Formation formation water and their petroleum geological significance, Dongying Sag.* Natural Gas Geoscience, 20: 603-609.

Rosenbaum, J. & Sheppard, S. 1986. *An isotopic study of siderites, dolomites and ankerites at high temperatures.* Geochimica et Cosmochimica Acta, 50: 1147-1150.

Sanyal, P., Bhattacharya, S. K. & Prasad, M. 2005. *Chemical diagenesis of Siwalik sandstone: Isotopic and mineralogical proxies from Surai Khola section, Nepal.* Sedimentary Geology, 180: 57-74.

Seewald, J. S. 2003. *Organic-inorganic interactions in petroleum-producing sedimentary basins.* Nature, 426: 327-333.

Spezzaferri, S., McKenzie, J. A. & Isern, A. 2002. *Linking the oxygen isotope record of late Neogene eustasy to sequence stratigraphic patterns along the Bahamas margin: results from*

a paleoceanographic study of ODP Leg 166, Site 1006 sediments. Marine Geology, 185: 95-120.

Sullivan, M. D., Haszeldine, R. S. & Fallick, A. E. 1990. *Linear coupling of carbon and strontium isotopes in Rotliegend Sandstone, North Sea: Evidence for cross-formational fluid flow.* Geology, 18: 1215-1218.

Tian, J. Q., Hao, F., Zhou, X. H., Zou, H. Y. & Peng, B. 2017. *Hydrocarbon generating potential and accumulation contribution of the fourth member of the Shahejie Formation in the Liaodong Bay sub-basin, Bohai Bay basin.* Marine and Petroleum Geology, 82: 388-398.

Wang, J., Cao, Y. C., Liu, K. Y., Liu, J., Xue, X. J. & Xu, Q. S. 2016. *Pore fluid evolution, distribution and water-rock interactions of carbonate cements in red-bed sandstone reservoirs in the Dongying Depression, China.* Marine and Petroleum Geology, 72: 279-294.

Xia, S. Q., Liu, J. Y., Liu, Z., Ye, D. Q, Chang, Y. Y., Gao, N. N., Li, H. & Liang, X. 2018. *The geophysical identification, characteristics, and petroliferous significance of sublacustrine fan deposits in the second member of Dongying Formation in Liaozhong Depression, Bohai Bay Basin.* Geological Journal, 53:692-706

Yang, Z., Zou, C. N., He, S., Li, Q. Y., He, Z. L., Wu, H. Z., Cao, F., Meng, X. L., Wang, F. R. & Xiao, Q. L. 2010. *Formation mechanism of carbonate cemented zones adjacent to the top overpressured surface in the central Junggar Basin, NW China.* Science China-Earth Sciences, 53: 529-540.

Yuan, G. H., Cao, Y. C., Zhang, Y. C. & Gluyas, J. 2017. *Diagenesis and reservoir quality of sandstones with ancient "deep" incursion of meteoric freshwater—an example in the Nanpu Sag, Bohai Bay Basin, East China.* Marine and Petroleum Geology, 82: 444-464.

Zhang, L. Y., Jiang, Y. L., Liu, H., Tan, L. J. & Zhang, L. 2003. *Relationship between source rock and oil accumulation in Dongying Sag.* Petroleum Exploration and Development, 30: 61-64.

Zheng, Y. F. & Chen, J. F. 2000. *Geochemistry of Stable Isotope.* Science Press, Beijing, China.

Zhu, G. Y. & Jin, Q. 2003. *Geochemical characteristics of two sets of excellent source rocks in Dongying Depression.* Acta Sedimentologica Sinica, 21: 506-512.

Zhu, G. Y., Qiang, Q., Zhang, S. C., Dai, J. X., Zhang, L. Y. & Li, J. 2004. *Distribution characteristics of effective source rocks and their control on hydrocarbon accumulation: a case study from the Dongying Sag, Eastern China*. Acta Geologica Sinica, 78: 1275-1288.

Received at: 22. 12. 2019
Revised at: 03. 02. 2020
Accepted for publication at: 21. 02. 2020
Published online at: 27. 02. 2020